August 1987 LRP 336/87

Contributed Papers presented at the

Workshop on
THEORY OF FUSION PLASMAS
Varenna, Italy - August 24-28, 1987

by the
Theory Group

COMPARISON OF NUMERICAL CALCULATIONS OF EXTERNAL KINKS WITH LARGE ASPECT RATIO THEORY

G. Schultz, F. Troyon, T. Tsunematsu*, A. Bondeson**, A. Roy
EURATOM/Switzerland Fusion Association,
Centre de Recherches en Physique des Plasmas,
Ecole Polytechnique Fédérale de Lausanne, CH-1007 Lausanne, Switzerland
**JAERI, Ibaraki-kên, Japan*
***on leave from Chalmers University of Technology, Sweden*

Abstract

The role of toroidicity for the structure of toroidal modes in tokamaks is investigated by examining circular cross-section equilibria with ERATO. Specifically we have examined a Shafranov step current profile, rounded off for numerical purposes, with $\beta = 0$. For $q_s < 2$ we find that detailed predictions of the inverse aspect ratio theory for the $n = 1$ external kink become invalid as R/a changes from 10 to 2.5. A Fourier-decomposition of the mode in poloidal mode number m shows that the $m = 2$ diagonal term in δW changes sign. With a conducting wall at $b/a = 1.5$ the lower aspect ratio equilibrium remains unstable for lower values of q_0 (> 1) and the unstable mode shows strong coupling of $m = 1$, 2 and 3. The radial plots of the $\delta W_{mm'}$ show a large cancellation in the diagonal terms. Analytically, $\delta W_{mm'}$, derived for low m modes by partial integration, reduces to Newcomb's expression in the large aspect ratio limit and resolves this large cancellation.

1. Introduction

Numerical calculations on MHD stability have as a side-effect provided an opportunity to study the relation between the standard Tokamak approximation technique of expanding in powers of inverse aspect ratio and the actual solutions. While it has been recognized very early that the global characteristics of the numerical solution of the eigenmode of the kink instability in a circular cross-section has the expected poloidal and radial structure, no detailed comparison has been made to our know-

ledge. This prompted us to re-examine a very simple problem studied by Shafranov [1] of the stability of a pressureless ($\beta = 0$) circular plasma of minor radius a, surrounded by a shell of radius b with a step current profile of radius r_0. This step current density profile $J(\Psi) \equiv dI/d\Psi$, where $I(\Psi)$ is the current flowing inside the Ψ surface, is rounded off for numerical reasons [2].

We consider the case met in simulations of disruptions in which the $q \approx 2$ surface becomes very cold, so that the outer region behaves like vacuum. We only investigate the most dangerous mode $n = 1$. The lowest eigenmode and the corresponding growthrate γ are calculated with ERATO [3].

Some results have already been reported in the case where there is no wall stabilization, namely $b = \infty$ [4]. The striking result was that an unstable mode, which we have named a "toroidal kink", looking very much like an internal kink except that it only exists with a free boundary, develops whenever $q_0 < 1$. In this paper we examine another aspect of the same problem, namely the external kink which exists in the range $q_0 > 1$, $q_s < 2$, and with a wall sufficiently close to the plasma to stabilize the weaker toroidal kink.

2. The stability of the external kink in the presence of a stabilizing shell

Since $q_0 > 1$ and $q_s < 2$ there is no singular surface in the plasma outside the central current core of radius r_0, so that the plasma radius a does not play any role in the stability boundary, although it naturally influences the growthrate and the mode pattern through the kinetic energy term. The stability condition of the kink in the large aspect ratio limit is found to be

$$q_0 \geq Q(b/r_0) = 1 + (\frac{r_0}{b})^4 \tag{1}$$

with only one parameter b/r_0. In the fully toroidal case we already know [4] that when $b = \infty$, there is no longer stability for any q_0, the internal kink being destabilized by coupling to the surface modes. There is then a continuous transition between the external kink at $q_0 > 1$ predicted by the large aspect ratio theory in leading order and the toroidal kink at $q_0 < 1$ which is only found in higher order. In order to have a comparison with the large aspect ratio calculation we take a value of b such that the "toroidal kink" becomes wall stabilized. A stability boundary such as (1) is then expected, but with an additional dependence on toroidicity, which can be expressed as a dependence on the current channel aspect ratio R/r_0. The property that, as far as stability is concerned, a current free, presssure free plasma layer with no singular surface inside it is equivalent to a vacuum region still holds in the toroidal case. The

stability limit is thus essentially independent of the plasma surface radius a, since the only effect which could lead to such a dependence is a slight non-circularity of the current channel which is not exactly circular when the plasma surface is circular. The stability limit can then be expressed as

$$q_0 > Q(\frac{b}{r_0}, \frac{R}{r_0}) \tag{2}$$

Figure (1) shows the stability limit obtained with $b/r_0 = 1.78$, a value sufficient to fully stabilize the internal kink. Aspect ratios vary from 12.2 to 3.1. The infinite aspect ratio limit (1) is 1.10. The stability limit drops towards $q_0 = 1$ as the aspect ratio decreases. The hardness of the instability decreases with the aspect ratio: The derivative at marginal stability $d\gamma^2/dq_0$ at the stability limit drops from 0.23 at the highest aspect ratio to less than 10^{-3} at the lowest.

3. Fourier analysis of modes and potential energy

ERATO contains a subroutine that Fourier-analyzes the eigenvector and the potential energy density with respect to the poloidal angle χ. This angle is defined through its relation to the arc length l along a meridian cut of a Ψ surface by

$$d\chi = \frac{B_\phi \, dl}{q|\nabla\Psi|} \tag{3}$$

where B_ϕ is the toroidal field [6].

A typical mode structure of an external kink is shown in figure 2 for an aspect ratio of $R/a = 2.5$ (corresponding to $R/r_0 = 3.1$), $q_0 = 1.04$ and $q_s = 1.8$. The wall in this case is at infinity and the square of the growthrate is $\gamma^2 = 2.1 * 10^{-3}$ [normalized to an Alfven transit frequency across the major radius]. The mode has a simple structure. The Fourier decomposition of the displacement normal to the magnetic surface shows the dominance of $m = 1$ in the center and $m = 2$ in the outer part of the plasma. There is a $m = 3$ component in the outer region with a small percentage of higher ms.

At larger aspect ratio the mode is a mixture of $m = 1$ and $m = 2$, the ratio of the $m = 3$ component to the $m = 2$ decreasing linearly as the inverse aspect ratio. At the largest aspect ratio $R/a = 10$ this ratio is never more than 5%.

The mode pattern behaves as expected. But the decomposition of the plasma potential energy density $d\delta W/ds$ (where $s = \sqrt{\Psi/\Psi_s}$, Ψ_s being the total flux in the plasma) reveals a more complicated behaviour. Table 1 shows the contribution of

the various Fourier components integrated over all flux surfaces to the total plasma potential energy.

$$\delta W = \sum_{m,m'} \delta W_{m,m'} \tag{4}$$

Only the lower half of the symmetric matrix is shown. The fact that the diagonal terms are all positive is unexpected. Since the mode is unstable the off-diagonal negative terms must offset the positive diagonal terms, even more so since the vacuum contribution is positive and large. The other surprise is that the diagonal $m = 3$ term is dominant. This is definitely at variance with the prediction of the large aspect ratio expansion which predicts a dominant negative diagonal $m = 2$ term.

The result of the same analysis at an aspect ratio of 5. is shown in Table 2. There $q_0 = 1.10$, and there is a wall at $b/a = 1.5$ in order to have a growthrate of the same order as in the other example. The $(2,2)$ contribution of the plasma is dominant and negative as expected. The same calculations repeated at other aspect ratios confirm that the loss of the dominance of the $(2,2)$ mode occurs between aspect ratios R/a of 5. and 2.5. But we have also noted by changing the current width at the aspect ratio $R/a = 2.5$ that no consistent pattern emerges, the $(2,2)$ component becoming sometimes destabilizing. Nevertheless, it appears that there is always a very strong stabilizing $(3,3)$ contribution. Thus although the first order coupling terms $(m, m \pm 1)$ are destabilizing at any aspect ratio, at small aspect ratio they are so strong that one cannot consider them as a perturbation.

The importance of the $m = 3$ and higher ms is nevertheless puzzling since the amplitude of the $m = 3$ relative to $m = 2$ remains small. The reason is a large cancellation of the $(2,2)$ potential energy in the radial integration of $d\delta W(2,2)/d\Psi$. It occurs for all diagonal terms. Figure 3 documents this cancellation for the same equilibrium as shown in figure 1 and Table 1. It shows that the positivity of $\delta W_{2,2}$ (Table 1) results from such a large cancellation. This cancellation exists also in the infinite aspect ratio limit but it is usually removed by an integration by parts on ξ_r, giving in the δW formulation the usual Shafranov expression with a surface term [5]. It has been a problem in all stability codes, especially when there are singular surfaces within the plasma such as when calculating internal kinks [7]. It is less severe in our case. It nevertheless explains why the dominance of the $m = 1$ and $m = 2$ components does not imply that higher m components can be discarded even though they are small.

4. Explicit cancellation of the diagonal term

We offer here a generalization applicable to toroidal configuration of the straight cylinder method of integrating by parts some terms in the energy principle to remove the dominant contribution from the diagonal term $\delta W_{m,m'}$. It is of no use to ERATO which does not rely on Fourier expansion of the eigenmode but it could improve the efficiency of PEST [6] or Degtyarev's code [8] in which the eigenvector is Fourier expanded.

We start from the standard ERATO expression for δW_p in the Ψ, χ coordinate system and we restrict the displacement to be incompressible, $\nabla \cdot \xi = 0$. The transverse displacement vector $\underline{\xi}$ is expressed in terms of 2 components X and V

$$\underline{\xi} = rX(\underline{\nabla}\chi \times \underline{\hat{e}}_\theta) + rV(\underline{\hat{e}}_\theta \times \underline{\nabla}\Psi)$$

To obtain the diagonal term m, X and V are replaced by ($I < 0$ in ERATO)

$$X(\Psi,\chi) = i\hat{X}(\Psi)e^{im\chi}\sqrt{\frac{q|I|}{T}}$$
$$V(\Psi,\chi) = \hat{V}(\Psi)e^{im\chi}$$

where $\hat{X}$ and $\hat{V}$ are chosen real. After integration by parts on the terms $\hat{X}\frac{d\hat{X}}{d\Psi}$, δW_p becomes

$$\delta W_p = \int_0^s d\Psi \{\frac{T^3}{q}(2\pi - \frac{n^2}{m^2}\frac{qI}{T})m^2|\hat{V} - \hat{V}_0|^2 + f_N(\frac{d\hat{X}}{d\Psi})^2 + g_N\hat{X}^2\} \quad (5)$$
$$- \pi\frac{\frac{T_s^2}{q_s^2}I_s(1 - \frac{n^2q_s^2}{m^2})}{(2\pi - \frac{n^2}{m^2}\frac{qI}{T})_s}\frac{d}{d\Psi}(\frac{qI}{T})_s\hat{X}_s^2$$

where $f_N = 2\pi\frac{T}{q}I^2\frac{(1 - \frac{nq}{m})^2}{2\pi - \frac{n^2}{m^2}\frac{qI}{T}}$

and

$$g_N = -I(m - nq)^2\{\frac{T^2}{q^2} < \frac{1}{r^4B_p^2} > + < \beta^2r^2B_p^2 > + (\frac{1}{m^2})\frac{\frac{T^3}{4q^3I}2\pi}{2\pi - \frac{n^2}{m^2}\frac{qI}{T}}[\frac{d}{d\Psi}(\frac{qI}{T})]^2\} +$$
$$- I\frac{dp}{d\Psi}\frac{d}{d\Psi} < r^2 > + \frac{IT}{2q}(1 - \frac{n^2q^2}{m^2})\frac{d}{d\Psi}[\frac{\frac{T}{q}2\pi}{2\pi - \frac{n^2}{m^2}\frac{qI}{T}}\frac{d}{d\Psi}(\frac{qI}{T})]$$
$$+ \frac{n^2}{m^2}\frac{I}{2\pi - \frac{n^2}{m^2}\frac{qI}{T}}\frac{d}{d\Psi}(\frac{qI}{T})\frac{dp}{d\Psi} < r^2 >$$

where the index s denotes surface quantities, $\beta \equiv \partial\chi/\partial\Psi|_n$, $< A > \equiv \int A\, d\chi$ and

$$V_0 \equiv -\frac{2(2\pi - \frac{n}{m}\frac{I}{T})\frac{qI}{T}\frac{d\hat{X}}{d\Psi} + (2\pi + \frac{n}{m}\frac{I}{T})\frac{d}{d\Psi}(\frac{qI}{T})\hat{X}}{2m(2\pi - \frac{n^2}{m^2}\frac{qI}{T})\sqrt{\frac{-qI}{T}}}$$

In the large aspect ratio limit for a circular plasma $\hat{X}$ reduces to the radial displacement ξ_r and

$$g_N = (m - nq)^2 8\pi^2 \frac{m^2 - 1}{m^2}$$

After minimisation over V, the expression for δW_p reduces then to the standard kink limit [5]. An examination of the terms in eq.(5) confirms that the surface term contains the leading terms and that the integral is of the same order as the coupling terms.

5. Conclusion

This study of external kinks in circular cross section Tokamaks at $q_s < 2$ has shown that while the stability limit and mode pattern are close to the predictions of the large aspect ratio theory, there are significant differences in the form of an aspect ratio dependence of the stability limit and dominant mode coupling effects at low aspect ratio, starting somewhere between 5 and 2.5. An expression of the diagonal terms of the plasma potential energy density Fourier analyzed in the poloidal angle has been given. It may be of some use in stability codes.

6. Acknowledgements

This work has been supported in part by the Swiss National Science Foundation.

m/m'	6	5	4	3	2	1	0
6	.087						
5	-.027	.483					
4	-.040	-.217	2.230				
3	-.025	-.250	-1.635	7.338			
2	-.013	-.133	-1.229	-9.752	3.206		
1	5.e-6	9.e-5	-.004	-.078	-1.569	1.	
0		2.e-5	7.e-5	-5.e-4	-.019	-.001	.020
-1			1.e-5	9.e-5	2.e-4	-1.e-4	-2.e-4

Table 1.

The plasma potential energy matrix $\delta W_{mm'}$, of an unstable kink for an equilibrium with $R/a = 2.5$, $q_0 = 1.04$, $q_s = 1.8$, $\gamma^2 = 2.1 * 10^{-3}$, $b = \infty$.

m/m'	6	5	4	3	2	1	0
6	4.e-4						
5	-1.e-4	.009					
4	-2.e-4	-.004	.172				
3	-1.e-4	-.006	-.170	2.393			
2	-2.e-4	-.004	-.148	-6.082	-45.486		
1	-1.e-6	-2.e-7	-3.e-4	-.015	-1.467	1.	
0		1.e-6	8.e-7	8.e-5	-.002	-.002	.004
-1			-1.e-6	1.e-6	-6.e-5	1.e-5	-2.e-5

Table 2.

The plasma potential energy matrix $\delta W_{mm'}$, of an unstable kink for an equilibrium with $R/a = 5$, $q_0 = 1.1$, $q_s = 1.7$, $\gamma^2 = 3.4 * 10^{-3}$, $b/a = 1.5$.

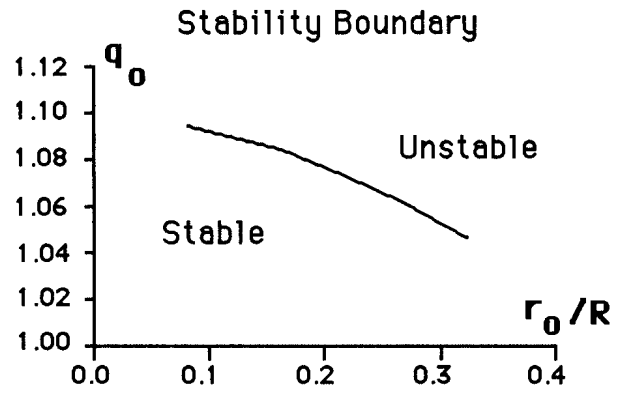

Fig. 1. The external kink stability boundary for $b/r_0 \approx 1.8$ as a function of inverse aspect ratio r_0/R. An increase of 3% in b/r_0 reduces q_0 by 1%.

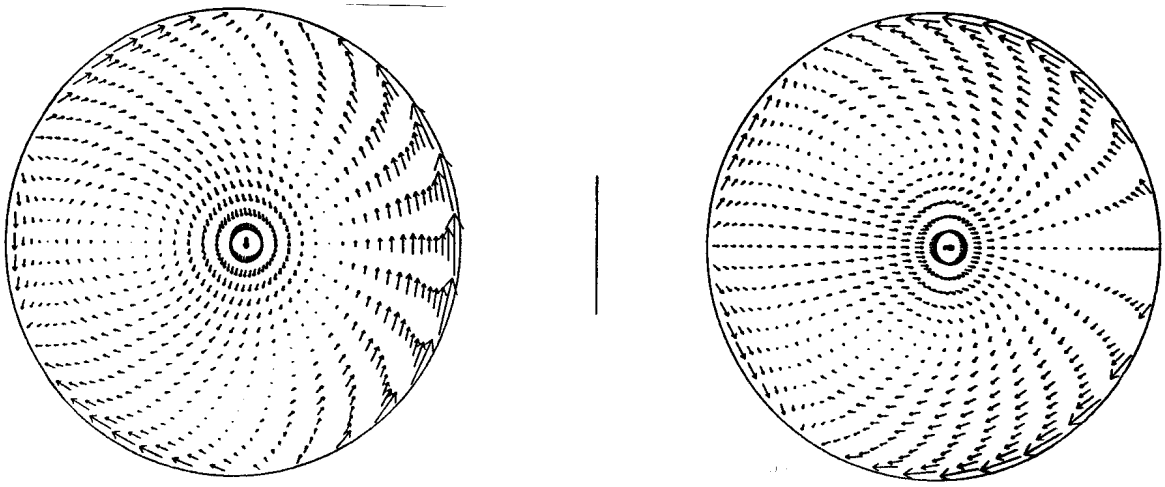

Fig. 2. The mode structure of an external kink at aspect ratio $R/a = 2.5$. The flow is shown in two meridian planes separated by 90°.

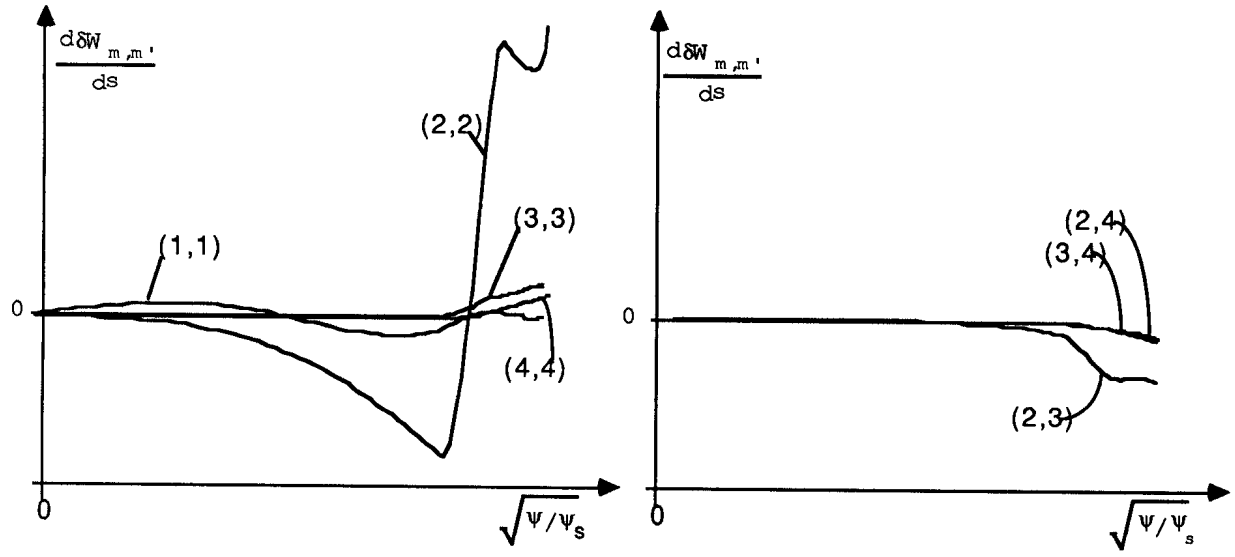

Fig. 3. The potential energy density of the most significant modes, $d\delta W_{mm'}/ds$, where $s \equiv \sqrt{\Psi/\Psi_s}$ is the radial parameter.

References

[1] Shafranov, V.D.: Sov. Physics - Techn. Phys. **15** (1970) 1751

[2] EUR-10418-EN International School of Plasma Physics "Piero Caldirola", Varenna, Italy, August 26–September 3, 1985: volume 1, p. 259

[3] Gruber, R., Troyon, F., Berger, D., et al.: Comp. Phys. Comm. **21** (1981) 323

[4] Turnbull, A., Troyon, F.: Europhysics Conference Abstracts – 12th European Conference on Controlled Fusion and Plasma Physics, Budapest, 2–6 September 1985, volume 9F, Part 1, p. 48

[5] Wesson, J.: Nucl. Fusion **18** (1978) 87

[6] Grimm, R.C. et al.: Methods of Computational Physics, Vol. **16**, 253

[7] Kerner, W., Gruber, R., Troyon, F.: Phys. Rev. Lett. **44** (1980) 536

[8] Degtyarev, L.M., et al.: Proc. Int. Conf. on Plasma Physics, Lausanne, Switzerland, 1984, vol. **I**, 157.

GCP STABILITY OF EQUILIBRIA WITH MASS FLOW

R. Iacono and A. Bondeson

Centre de Recherches en Physique des Plasmas
Association Euratom - Confédération Suisse
Ecole Polytechnique Fédérale de Lausanne
21, Av. des Bains, CH-1007 Lausanne / Switzerland

ABSTRACT

The effect of mass flows on ideal stability of cylindrical equilibria is investigated using both the magnetohydrodynamic (MHD) and guiding center (GCP) plasma models.The flows modify the local criterion for instability at the resonant surface where $\underline{k}\cdot\underline{B}=0$. A stability limit is found in the MHD picture at a critical velocity where the shear of the flow balances the propagation of the slow wave along the magnetic field. Just below the critical velocity there is instability independent on the pressure gradient. Above the critical speed the Suydam modes are stable, but an infinite sequence of unstable modes still exists with frequencies accumulating toward the edge of the slow wave continuum at non zero Doppler shifted frequency.

The stability limit is removed in the guiding center model, due to the more realistic kinetic treatment of the parallel motion, which smooths the resonance between flow and sound waves. Numerical results for a simple test case are presented, showing that in the GCP model sheared equilibrium flows can stabilize localized modes.

I INTRODUCTION

A common feature of some recent works on ideal MHD stability of equilibria with flows is the appearance of a new destabilizing effect associated with a resonance between equilibrium flows and the slow wave. This resonance occurs in cylindrical geometry in the generalized Suydam criterion for the stability of local modes in the presence of sheared axial or azimuthal equilibrium flows [1]. The same resonance is found in axisymmetric toroidal geometry in a sufficient condition for stability of ballooning modes [2]. In this case the analysis is restricted to a general field aligned flow, due to the failure of the usual ballooning representation in the case of sheared toroidal flows [3].

However, since the slow wave is essentially an ion sound wave along the field lines, and sound waves in collisionless (i.e. typical tokamak) plasmas are treated incorrectly in the MHD model, it is very likely that modifying the modeling equations to include wave-particle resonance would change drastically the picture.

One way to treat more accurately the parallel dynamics without completely loosing the simplicity of a fluid description is offered by the guiding center plasma model (GCP) formulated by Grad [4]. Here the plasma behaviour perpendicular to the magnetic field is described by fluid MHD-like equations, while a one dimensional collisionless kinetic equation governs the parallel motion.

An application of this model to study the stability of static equilibria in cylindrical geometry was made by Pao [5], who derived the second order radial eigenvalue problem, similar to the Hain-Lüst (HL) equation [6] and obtained the corresponding modified Suydam criterion for local stability . Tataronis and Grossmann [8] derived a system of two first order coupled equations (corresponding to the MHD system of Appert, Gruber and Vaclavik [7]) and used the GCP model to describe RF absorption in a non uniform plasma. The similarity of GCP model to MHD is readily seen from Ref. [5,8]. For instance, for a Maxwellian isothermal distribution the GCP criterion for local stability reduces to the Suydam criterion and the properties of the Alfvén waves (but not the slow waves!) are very similar in the GCP and MHD models.

However very essential differences between the two models are found when equilibria with sheared mass flows are considered, leading to almost opposite conclusions. The purpose of the present work is to formulate the GCP stability problem for cylindrical equilibria with arbitrary flows and to make a first comparison with the corresponding MHD picture.

The paper is organized as follows : in Sec. II we recall some of the results obtained in Ref. [1], where the MHD radial eigenvalue problem is derived and the main effects of

flow on stability of local modes are discussed. The basic equations of the GCP model are presented in section III. In Sec. IV the second order radial eigenvalue problem for the GCP model for general equilibrium flows is derived and compared with the corresponding MHD problem. Finally in Sec. V a simple numerical test case is used to compare MHD and GCP predictions concerning the stability of localized modes . The first numerical results show that the complete breakdown of stability in the MHD model at the sound speed is removed in the GCP picture. In contrast, in the GCP model local modes are stabilized when the sheared axial equilibrium flow is increased.

II MHD PICTURE

The MHD stability problem for a cylindrical plasma in the presence of general equilibrium flows was formulated in Ref. [1]. The linearized MHD equations reduce to a pair of first order radial differential eqution s for the radial displacement ξ_r and the total perturbed pressure p_* . This system has the same structure as the static eigenvalue problem [7]. Flows modify the coefficients and, in particular, axial flows only enter through the Doppler shifted frequency $\tilde{\omega} = \tilde{\omega}(r) = \omega + \underline{k}\cdot\underline{V}$. Here $\underline{V}$ is the equilibrium velocity field and an $\exp[i(\omega t + \underline{k}\cdot\underline{r})]$ dependence has been assumed for the perturbed quantities.

An indicial equation analysis was used to study the stability of modes localized around the resonant surface $r=r_0$ where $k_{||}=0$ at the marginal point $\tilde{\omega}(r_0)=0$ and a modified Suydam criterion was derived. In the case of purely axial flow the local criterion for instability takes the simple form

$$\left(\frac{q}{q'B_z}\right)^2 \frac{2}{1-M^2}\left(-\frac{p'}{r}+\frac{2\beta M^2}{\beta - M^2}\frac{B_\theta^2}{r^2}\right) > \frac{1}{4} \qquad (1)$$

where $M^2 \equiv \rho(\tilde{\omega}'/F')^2$, $F \equiv \underline{k}\cdot\underline{B}$, $\beta \equiv \gamma p/(\gamma p + B^2)$, $q=rB_z/RB_\theta$ is the safety factor, R the major radius and the prime means derivative w.r.t. the radius. The condition $M^2=\beta$ defines a critical velocity where the shear of the convection exactly balances the propagation of the slow wave along the field lines. We see that subcritical ($M^2<\beta$) axial flows decrease the maximum pressure gradient which can be stably confined and at the critical speed there is instability independent of the pressure gradient.

The pessimistic picture is completed when supercritical flows are considered.

Above the critical velocity the $\underline{k}\cdot\underline{B}=0$ surface becomes indeed stable; but the infinite sequence of unstable modes is now connected with the edge of the slow wave continuum, which passes through the resonant surface exactly at the critical speed. The existence of a stability treshold at the critical velocity $M=\beta^{1/2}$ and the destabilization of the slow wave continuum for supercritical velocities are the two main new effects which emerge from the MHD model. We refer to Ref. [1] for a more detailed analytic and numerical study of these effects.

III GCP BASIC EQUATIONS

In the GCP model the plasma is considered to consist of electrons and one kind of positive ions with distribution functions $f^{\pm}(\mu, v, \underline{x}, t)$ where μ is the magnetic moment and v the particle velocity along the magnetic field. The densities $\rho^{\pm}$, the macroscopic parallel velocities $V_{||}^{\pm}$ and the pressure components $p_{||}^{\pm}$, $p_{\perp}^{\pm}$ for the two species are computed by taking moments of $f^{\pm}$:

$$[\,\rho,\, V_{||},\, p_{||},\, p_{\perp}\,]^{\pm} = \int [\,1,\, v,\, v^2,\, \mu B\,]\, f^{\pm}\, d\mu dv \qquad (2)$$

and the corresponding fluid quantities ρ, $V_{||}$, $p_{||}$, $p_{\perp}$ are obtained by summing over electrons and ions.The total pressure tensor is

$$\underline{\underline{P}} = \Delta\, \underline{B}\,\underline{B} + p_{\perp}\, \underline{\underline{I}} \qquad (3)$$

where $\Delta \equiv (p_{||}-p_{\perp})/B^2$ and $\underline{\underline{I}}$ is the unit tensor. The macroscopic description is then completed by the following MHD-like equations for the magnetic field $\underline{B}$ and the perpendicular velocity $\underline{u}$:

$$\rho(\partial_t + \underline{V}\cdot\nabla)\underline{V} = -\nabla\cdot\underline{\underline{P}} + (\nabla\times\underline{B})\times\underline{B} \qquad (4)$$

$$\partial_t \underline{B} = \nabla\times(\underline{u}\times\underline{B}) \;,\quad \nabla\cdot\underline{B} = 0 \qquad (5)$$

where $\underline{u} = \underline{V} - V_{||}\hat{b}$, $\hat{b} = \underline{B}/B$, $\underline{V}$ is the total macroscopic velocity and ∂_t means derivative w.r.t. time.

The motion of the particle guiding centers is governed by one dimensional kinetic equations along the magnetic field lines

$$\partial_t f^{\pm} + V\cdot[(\underline{u}+v\hat{b})f^{\pm}] + \underline{\kappa}\cdot\underline{u}\,\partial_v(vf^{\pm}) + [(e/m)^{\pm}\,\hat{b}\cdot\underline{E} - \hat{b}\cdot\nabla(\mu B - u^2/2)]\,\partial_v f^{\pm} = 0 \qquad (6)$$

where $\underline{\kappa} \equiv \hat{b}\cdot\nabla\,\hat{b}$ is the magnetic field curvature, $e^{\pm}$ and $m^{\pm}$ are respectively charge and

mass of ions and electrons and $\underline{E}$ is the electric field. Consistency requirements of the theory [4] give the additional constraint $V_{||}^{+} = V_{||}^{-}$. Using this condition the following expression for the parallel electric field can be obtained

$$[(e/m)^{+}+(e/m)^{-}]\hat{b}\cdot\underline{E} = (\hat{b}\cdot\nabla\cdot\underline{\underline{P}}/\rho)^{+} - (\hat{b}\cdot\nabla\cdot\underline{\underline{P}}/\rho)^{-} \qquad (7)$$

IV GCP RADIAL EIGENVALUE PROBLEM

Linearizing the GCP equations (4)-(5) and expressing the perturbed quantities in terms of the Lagrangian displacement $\underline{\xi}$ we obtain the following equation of motion

$$-\rho\tilde{\omega}^2\underline{\xi} = -(\nabla\cdot\underline{\underline{P}})^1-\nabla(\underline{B}\cdot\underline{Q})+\underline{B}\cdot\nabla\underline{Q}+\underline{Q}\cdot\nabla\underline{B}+2i\tilde{\omega}\rho(V_\theta/r)\underline{\xi}\times\hat{z} \qquad (8)$$

$$-[(\rho V_\theta^2/r^2)\ \nabla\cdot\underline{\xi}+\xi_r(\rho V_\theta^2/r^2)']\underline{r}$$

(From now on we will indicate the perturbed quantities with a superscript 1).
In the general case where the equilibrium is anisotropic, the following expression can be derived

$$(\nabla\cdot\underline{\underline{P}})^1 = \nabla p_\perp^{\,1} + \Delta[iF(\underline{Q}+\xi_r\underline{B}'+\xi_r\underline{B}_\theta/r)-2(B_\theta Q_\theta/r^2)\underline{r}] - \Delta^1(B_\theta^2/r^2)\underline{r} \qquad (9)$$

$$+\underline{B}(iF\Delta^1+\xi_r\Delta')$$

where $\Delta=(p_{||}-p_\perp)/B^2$ and $\Delta^1=(p_{||}^{\,1}-p_\perp^{\,1}-2\Delta\underline{B}\cdot\underline{Q})$.

In analogy with the MHD case we define $p_* = p_\perp^{\,1}+\underline{B}\cdot\underline{Q}$. We give here for completeness the equilibrium equation

$$(p_\perp + B^2/2)' = (\rho V_\theta^2 - \sigma B_\theta^2)/r \qquad (10)$$

where $\sigma = 1 - \Delta$.
The reduction of (8) to a radial eigenvalue problem can then be done essentially like in the MHD model, once $p_\perp^{\,1}$ and $p_{||}^{\,1}$ are expressed in terms of p_* and ξ_r. To do that we linearize the kinetic equation (6), obtaining for the perturbed distribution function

$$f^{1\pm} = -\xi_r\partial_r f^{\pm} + \{(\underline{B}\cdot\underline{Q}+\xi_r BB')/B^2\}[f^{\pm}+\mu B\partial_v f^{\pm}/(v-w)]$$

$$+ (i/BF)\{B^2[(e/m)^{\pm}\hat{b}\cdot\underline{E}+\hat{b}\cdot\nabla(u^2/2)]^1+v(\underline{\mu}\cdot\underline{B}\cdot\nabla\underline{B})^1\}[\partial_v f^{\pm}/(v-w)] \qquad (11)$$

where $w = -(\omega+\underline{k}\cdot\underline{\mu})/k_{||}$.

The values of $p_{||}^{\,1}$ and $p_\perp^{\,1}$ are then computed by taking the corresponding moments of $f^{1\pm}$.

We obtain

$$p_{||}{}^1 = (\underline{B}\cdot\underline{Q}+\xi_r BB')(\Delta+B\tilde{\omega}^2\Theta_2/F^2) - \xi_r[p_{||}'+X^2(B^2\tilde{\omega}^2\Theta_3/F^2-\rho)/r] \qquad (12)$$

$$p_* = (\underline{B}\cdot\underline{Q}+\xi_r BB')K + \xi_r H/r \qquad (13)$$

where $K=1+2p_\perp/B^2+\Theta_1$, $X^2=(FV_\theta-\tilde{\omega}B_\theta)^2/F^2$, $H=\sigma B_\theta{}^2-\rho V_\theta{}^2-BX^2\Theta_2$ and the Θ_i, $i=1,2,3$ are complex functions involving integrals of the equilibrium distribution functions of the form

$$J(l,n) = \int_{-\infty}^{\infty}\frac{dv}{v-w}\int_0^{\infty} d\mu\,\mu^l\left\{\left(\frac{1}{\rho^n}\frac{\partial f}{\partial v}\right)^+ + (-1)^n\left(\frac{1}{\rho^n}\frac{\partial f}{\partial v}\right)^-\right\} \qquad (14)$$

The explicit expression for the Θ_i can be found in ref. [5,8]. Using the expression of $p_{||}{}^1$ and $p_\perp{}^1$, the radial eigenvalue problem for the GCP model can finally be derived

$$(r\xi_r)'/r = b_1\xi_r - b_2 p_* \qquad (15)$$

$$p_*' = b_3\xi_r - b_1 p_*$$

where

$$b_1 = (1/rB^2)[B_\theta{}^2 + H/K - 2EB_z T/A], \qquad b_2 = (1/K - E^2/A)/B^2,$$

$$b_3 = A - [(\rho V_\theta{}^2-\sigma B_\theta{}^2)/r^2]' + (B_\theta{}^2/r^2B^2)(\sigma B_\theta{}^2-\rho V_\theta{}^2)$$

$$+(1/r^2B^2)[H^2/K - 4B_z{}^2T^2/A + X^2(\rho B_\theta{}^2-B^2X^2\Theta_3) + 2B_\theta{}^3T/F]$$

and

$$A = \rho\tilde{\omega}^2-\sigma F^2, \quad E = \hat{r}\cdot\underline{k}\times\underline{B} = mB_z/r+k_z B_\theta, \quad T = (\sigma FB_\theta - \rho\tilde{\omega}V_\theta).$$

The MHD eigenvalue problem can be recovered from (15) once the following formal identifications are made:

$$\sigma \to 1, \quad K \to S/s, \qquad B\Theta_2 \to \gamma p\rho F^2/s, \qquad \Theta_3 \to \rho^2F^2/s \qquad (16)$$

where

$$S = (\gamma p+B^2)\rho\tilde{\omega}^2 - \gamma pF^2, \quad s = B^2\rho\tilde{\omega}^2 - \gamma pF^2.$$

Note that $K=0$ ($S=0$) is the dispersion relation for slow waves in the GCP (MHD) model. An important difference between the GCP and MHD pictures can be seen from the compression term. The GCP result is

$$\nabla\cdot\underline{\xi} = -\frac{\rho+B\Theta_2}{\rho B^2 K}\left\{ p_* + \frac{\xi_r}{r}\left[\rho V_\theta^2 - \sigma B_\theta^2 + X^2\left(B\Theta_2 \frac{B^2\Theta_3 K}{\rho+B\Theta_2}\right)\right]\right\} \qquad (17)$$

while the MHD expression is

$$\nabla\cdot\underline{\xi} = -\frac{\rho\tilde{\omega}^2}{S}\left\{ p_* + \frac{\xi_r}{r}\left[\rho V_\theta^2 - B_\theta^2 - X^2\frac{F^2}{\tilde{\omega}^2}\right]\right\} \qquad (18)$$

Let us examine the behaviour of eq. (18) at the resonant surface $k_{||}=0$ when $\tilde{\omega}=0$. It is easy to show that, due to the division by S, $r\nabla\cdot\underline{\xi}/\xi_r$ grows without bounds when the resonance condition $\rho(\tilde{\omega}'/F')^2=\gamma p/(\gamma p+B^2)$ (which is the same resonance appearing in the Suydam criterion (1)) is approached. On the other hand we see that in the GCP expression (17) S is replaced by K and the resonance is smoothed , due to the complex part of the kinetic integrals.

In the next section we will study numerically the influence of this damping of the slow waves on the stability of localized modes.

V NUMERICAL RESULTS

The eigenvalue spectrum of the MHD system was studied numerically in Ref. [1]. As the resonant speed was approached, two sequences of Suydam modes , with different behaviour, could be identified. The first sequence remained unstable above the critical speed where the unstable modes were transformed into discrete slow waves. The second sequence was stabilized aroud the critical speed. For both type of modes, overlap with continua at other radial locations played a decisive role for the stability . The main result of Ref. [1] is that the sound speed sets an upper limit for MHD stability, all equilibria with near or super critical flow being unstable.

Similar numerical techniques have been applied in a preliminary study for the GCP model. For a fair comparison, we took the same equilibrium as in the MHD calculation and assumed that the plasma was isothermal ($P_e=P_i$) and isotropic ($p_{||}=p_\perp$). For the evaluation of the kinetic integrals we used a Maxwellian distribution function for the ions and the electrons were assumed to be massless, $m_e\rightarrow 0$, so that the electrons satisfied the Boltzmann distribution.

The important difference between the MHD and GCP results can be seen comparing

the stability diagrams for the two cases, which are presented in fig. (1) and (2). There P_1 measures the pressure gradient and v_{z_o} is the axial plasma flow. The MHD stability diagram refers only to the existence of localized instabilities (i.e. infinite sequencies of unstable modes) whereas the GCP diagram was computed by following the most unstable eigensolution as the pressure and flow speed were varied. It has been verified for a few points in the region marked stable in the GCP diagram by means of Nyquist plots that there is no eigensolution with growth rate larger than 10^{-5}. These studies strongly indicate that is sufficient to follow the eigenmode that is most unstable in the static case . Another interesting result is that the infinite sequences of instabilities are destroyed by sheared mass flow in the GCP model,contrary to the MHD case.

In conclusion, we find that the stability of the localized modes looks very different within the MHD and GCP models.Whereas MHD predicts complete loss of stability for near sonic flows, the GCP model predicts that flow is stabilizing for the localized modes. In both cases, the effect of the flow is strong because of resonance with the slow waves, which in the MHD model become unstable but in the GCP model are strongly Landau damped. The GCP result is thus very optimistic for stability of rotating plasmas,although we have not yet studied several important aspects such as the influence of flow on kink modes, effect of curvature of the flow, etc.

REFERENCES

[1] A. Bondeson, R. Iacono and A. Bhattacharjee, Phys. Fluids 30, 2167 (1987)

[2] A. Bhattacharjee, R. Iacono and C. Paranicas, submitted to Phys. Rev. Lett.

[3] E. Hameiri and P. Laurence, J. Math. Phys. 25, 396 (1984)

[4] H. Grad,in Electromagnetics and Fluid Dynamics of Gaseous Plasma(Proc.Symposium), Polytechnic Press, Brooklyn, New York (1961)

[5] Y.P. Pao, Nucl. Fusion 14, 25 (1974)

[6] K. Hain and R. Lüst, Z. Naturforsh. 13a, 936 (1958)

[7] K. Appert, R. Gruber and J. Vaclavik, Phys. Fuids 17, 1471 (1974)

[8] J.A. Tataronis and W. Grossmann, Nucl. Fusion 16, 667 (1976)

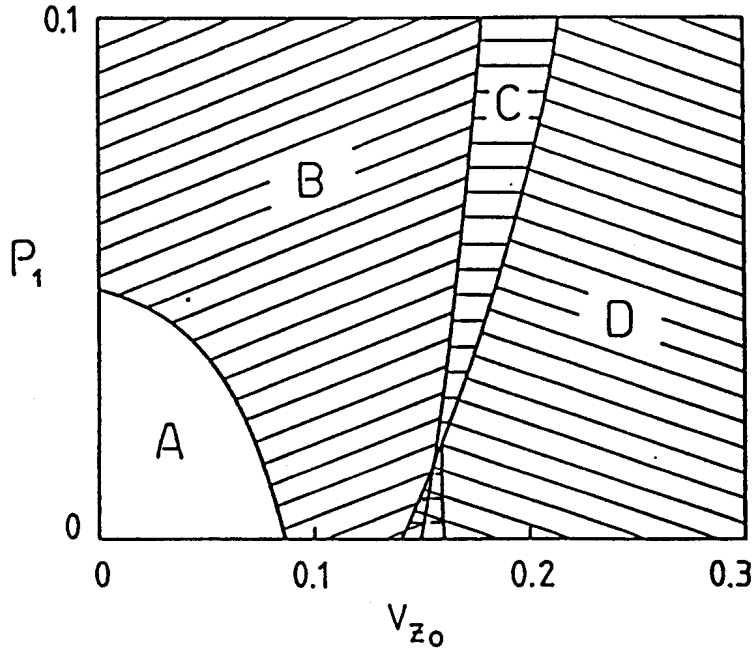

Fig. 1. MHD stability diagram. Region A is stable according to the local criterion, region B is unstable to the modified Suydam modes, regions C and D are unstable to discrete slow modes. The boundary between B and C corresponds to the critical velocity $M^2 = \beta$.

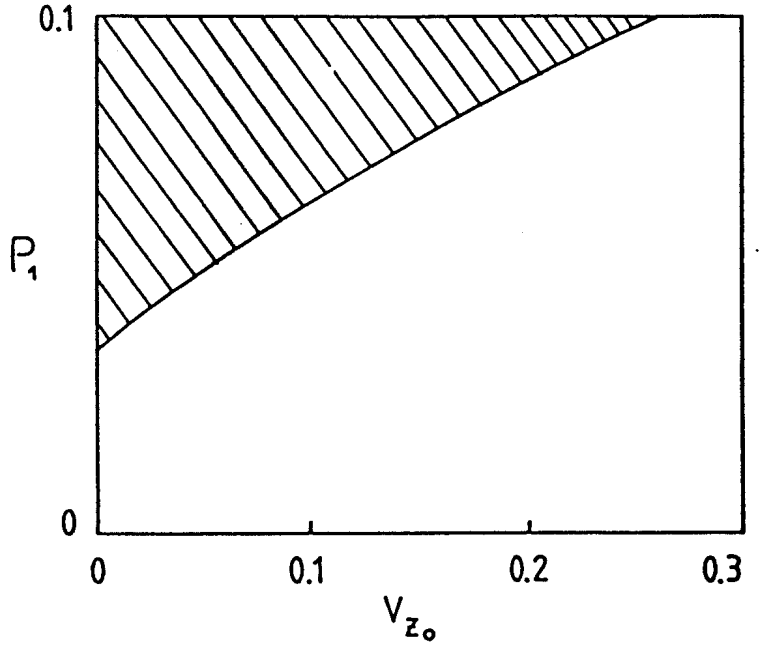

Fig. 2. GCP stability diagram. The hatched region is unstable. Note that the stable pressure gradient increases with flow.

NUMERICAL STUDY OF BALLOONING STABILITY FOR QUASI DIVERTOR TOKAMAK EQUILIBRIA

A. Roy and F. Troyon

Centre de Recherches en Physique des Plasmas
Association Euratom - Confédération Suisse
Ecole Polytechnique Fédérale de Lausanne
21, Av. des Bains, CH-1007 Lausanne / Switzerland

ABSTRACT

The predictions of C.M. Bishop et al. [1, 2] relative to the influence of a separatrix on ideal MHD ballooning stability are verified for a class of quasi-circular plasmas of aspect ratio 3.7 with variable current profiles. Self-consistent equilibria are generated with a given flux-average current profile and a flat pressure profile in a fixed central region. The pressure gradient is pushed iteratively in the outer region until it reaches the first stability limit if there is one, or is increased progressively, if there is coalescence of the first and second stability region, until numerical difficulties arise. The dependence of the coalesced region on the various parameters (current density at the edge, total current, poloidal location of the X-point) is given.

1 INTRODUCTION

Coalescence of the first and second regions of stability of ideal MHD ballooning modes offer interesting prospects for circular or quasi-circular tokamaks which have very low β limits in the first region of stability. The possibility of having such a coalescence inside the plasma, in an intermediate range of magnetic surfaces between the core and the surface, has been demonstrated by a number of authors using carefully taylored current profiles [3,4]. C.M. Bishop [1,2] has recently shown that in a single null divertor quasi-circular configuration it is possible to have coalescence at the separatrix and in its immediate vicinity, provided that the X-point is directed vertically or towards the major axis and the current density on the separatrix

exceeds a threshold value. This offers the possibility of creating plasmas in which there is coalescence over a wide range from the separatrix inward.

We have made numerical studies to verify some of these predictions, in particular, the constraint on the current density and the influence of the poloidal location of the X-point, and to exhibit very high β stable equilibria in which the pressure gradient is located mainly at the edge in a region of strong shear thus maybe alleviating the risk of infernal modes. These are first results to verify the trend and do not cover an extensive parameter range.

2 PARAMETRISATION OF EQUILIBRIA

The plasma shape is parametrized in the following way :

$$\begin{aligned} r &= R(1 + a\rho(\alpha)\cos\alpha) \\ z &= Ra\,\rho(\alpha)\sin\alpha \\ \rho(\alpha) &\equiv 1.0 + \sigma\Delta/\{\Delta + (\sin^2((\alpha-\alpha_0)/2) + \varepsilon\}^{\gamma} \end{aligned} \qquad (1)$$

where R is the major radius, α is a parameter which varies between 0 and 2π, a is the inverse aspect ratio when $\sigma=0$, α_0 is a free parameter which determines the orientation of the X-point, σ is the parameter which gives the size of the "bump" of the surface due to the proximity of the X-point and Δ, ε, γ are three parameters which fix the width of the bump and give some possibility to adjust its shape also. This plasma surface is not exactly a separatrix but it can be considered as being just inside a single null separatrix.

The aspect ratio a^{-1} of the undeformed circular plasma is kept fixed at 3.7.

The average current density profile has the form

$$J(\psi) = \frac{\oint \frac{J_\phi\, dl}{r\, B_P}}{\oint \frac{dl}{r\, B_P}} = J_S + J_S\,(1-J')\,(1-\psi/\psi_S) \qquad (2)$$

where r is the distance to the major axis, J_ϕ is the toroidal current density, B_p the

poloidal field and the integral is along a poloidal field line. The poloidal flux is normalized in such a way that ψ=0 on the magnetic axis and its value at the plasma surface is denoted ψ_s. The parameter J' controls the current peaking (ratio of current density at the axis and the plasma surface) and thus the shear q_l/q_0, where

$$q_l \equiv 2B_0 / RJ_{av} \qquad (3)$$

is the cylindrical q and q_0 the safety factor on axis. In eq. (3) B_0 is the vacuum toroidal field at the major radius R, and J_{av} is the current density averaged over the full cross-section S(J_{av}≡I/S).

Since we wish to study the influence of the separatrix we limit the range where $dp/d\psi \neq 0$ to a shell

$$0.4\psi_s < \psi < \psi_s \qquad (4)$$

The initial $dp/d\psi$ profile is represented as a third order polynomial for $0.4\psi_s < \psi < 0.8\psi_s$ and constant for $0.8\psi_s < \psi < \psi_s$, imposing the additional constraint that $d^2p/d\psi^2$ at $\psi = 0.4\psi_s$ and $0.8\psi_s$. It is also chosen sufficiently low to lie below the limit of the first region of stability if there is one.

The ballooning criterion is then checked on a number of surfaces and $dp/d\psi$ is modified iteratively on each of these surfaces according to a procedure to be described below.

The equilibrium is found at each step by solving the Grad-Shafranov equation by a finite-element code CLIO described elsewhere [5] ,it is a quasi inverse code ,therefore no mapping is necessary to compute the coefficients of the ballooning equation.

3 THE ITERATION ON dp/dψ

The ballooning criterion [6] used in these studies has the form

$$\delta W = \int_{-\infty}^{\infty} d\theta \left\{ A \left(\frac{\partial X}{\partial \theta} \right)^2 + \frac{dP}{d\psi} K X^2 \right\} \qquad (5)$$

where X is related to the normal displacement ξ_n by

$$X = \frac{r\,B_\rho}{T}\,\xi_n \tag{6}$$

and the two coefficients $A(\psi,\theta)$, $K(\psi,\theta)$ are equilibrium quantities :

$$A(\psi,\theta) = \frac{T^2}{r^4 B_\rho^2 \mathcal{J}}\left[1 + \left(\frac{\mathcal{J} r^2 B_\rho^2 G}{B}\right)^2\right]$$

$$K(\psi,\theta) = -2\frac{r^2}{B^2}\left[\frac{\partial(P + B^2/2)}{\partial\psi}\bigg|_n - \frac{T^2 G}{r^2 B^2}\frac{\partial(B^2/2)}{\partial\theta}\right] \tag{7}$$

where B is the total magnetic field, $T \equiv rB_\phi$, and

$$\mathcal{J} = \frac{\rho\, B_\varphi}{\partial\psi/\partial s} \quad ; \quad G = \frac{\partial\theta}{\partial\psi}\bigg|_n + \frac{1}{\mathcal{J}}\int_{\theta_0}^{\theta}\frac{\partial\mathcal{J}}{\partial\psi}\bigg|_{\theta'} d\theta' \tag{8}$$

ρ is the distance to the magnetic axis, the angle $\theta_0(\psi)$ is the usual free parameter which must be varied. A is positive definite while K changes signs. The vector X is expanded in linear finite elements and the signature of δW is determined on every ψ surface for values of θ_0 ranging from 0 to 2π. This gives a yes or no answer to ballooning stability.

The iteration scheme chosen consists of multiplying at each step $dp/d\psi$ of the previous step by a constant factor C, recompute the equilibrium and test the ballooning criterion. If all surfaces are stable the process is repeated until one of two possibilities occur.

The first possibility is that the ballooning criterion becomes violated on one surface. The value of $dp/d\psi$ is then corrected to be marginal on that surface. The fact that the equilibrium code uses finite elements, with radial nodal points reset at each step such that they form a rectangular mesh in the (ψ,θ) plane, facilitates greatly the procedure. The step is then repeated from this new initial state by multiplying again

$dp/d\psi$ by C on every surface and bringing it back to its marginal value if it exceeds it in a certain range. If there is no coalescence of the first and second stability regions the scheme will lead to a sequence of equilibria of increasing β, marginal over a growing range of magnetic surfaces. It would eventually converge to a fully marginal equilibrium with a discontinuity of $dp/d\psi$ at the transition point $\psi=0.4\psi_s$ since $dp/d\psi$ is forced to vanish there. The procedure is stopped before the discontinuity builds up because of numerical problems encountered in resolving
the equilibrium equation. There always remains a small range near the transition point which is not optimized.

The second possibility is that the pressure gradient is limited by the ballooning criterion only in a fraction of the plasma while no limit is encountered in the rest of the plasma for a number of iterations, until numerical problems in the calculation of the equilibrium prevent further iteration. We interpret this as coalescence of the first and second stability regions. In practice, the value of ψ at which there is the transition to coalescence is very clearly seen. The difficulties which limit the increase in pressure are numerical since it is possible to increase the number of iterations, and thus the pressure, by decreasing the size of the step measured by the factor C and by increasing the resolution of the equilibrium. The values of β obtained so far, in cases where there is coalescence in part of the plasma, have been limited by the maximum resolution possible and by the lowest value of C used in these calculations , 1.03.

In this iterative scheme it is not possible to find an equilibrium in the second stable domain when there is no coalescence.

4 RESULTS

The first case (figure 1) has an outside bump ($\alpha_0=45^0$) and a moderatly peaked current profile profile, $J'=1.25$ (eq.2). The current corresponds to $q_l=1.36$. It is found that the pressure gradient is limited everywhere except maybe very close to the inner limit at $0.4\psi_s$ by the first stability boundary. This is not in contradiction with the known results [3,4] , namely that coalescence is possible in a circular plasma in an intermediate region, but in our case coalescence appears outside the shell where $p'\neq 0$. Peaking more the current to obtain a more realistic profile does

not introduce coalescence but instead pushes further inward the region of coalescence. Thus the separatrix has not introduced coalescence at the surface, at least for monotonic q profiles, in agreement with reference 1.

Coalescence is also not visible if the bump is at $\alpha_0=0^o$ and even if the current profile is flat , J'=1.0.

The case studied most is the inner X-point ($\alpha_0=180^0$) with σ= 0.9 , Δ= 0.2 ,ε=0.002 , and γ= 0.5 . A scan over the total current I and the current peaking factor J' has been made . Coalescence occurs between the plasma surface and another surface labeled ψ_c .The dependence of ψ_c on the normalized current $I_E=\mu_0 I/RB$ and on the current peaking factor represented as the ratio of the current densities at the axis and the plasma surface is shown in fig. 2 . For comparison the limit of coalescence for one value of the normalized current I_E=0.3 is shown on the same figure for two different orientations of the bump, $\alpha_0=135^o$ and 90^o. There does not seem to be much difference. More such studies near the transition angle of 90^o are needed. The curve for $\alpha_0=90^o$ does give a clue as to how the transition might occur.

Figure 3 and 4 show two high beta equilibria with $\alpha_0=180^o$ and $\alpha_0=90^0$, and fully stable against ballooning modes. In those two cases the initial pressure gradient profile was zero in a smaller fraction of flux surfaces than described before , the reason for that is to demonstrate that coalescence of the two region of stability occurs over a large fraction of the plasma cross section.

5 CONCLUSIONS

The calculations made so far support the two main predictions of C.M. Bishop et al., namely: a separatrix with an X-point can cause coalescence of the first and second regions of ballooning stability in its vicinity if the X-point is located inward or vertically; a threshold current density on the separatrix is needed for this coalescence to occur.

In these calculations the influence of the separatrix extends sufficiently deep into the plasma to allow coalescence over 60% of the plasma cross-section, measured in terms of poloidal flux.

There does not appear to be, in the cases studied so far, a significant difference

in the threshold current density for coalescence when the X-point is located inside at $\alpha_0=180^o$, at 135^o or at 90^o.

In cases where coalescence has been achieved, the highest β has been limited by the resolution of the equilibrium code, which limits the pressure gradient and by the running time necessary to increase the pressure sufficiently slowly to have the equilibrium code converge at each step.

These calculations have been done with a fixed current density profile and not as usually done with a fixed q-profile. The next step will be to increase the peaking of the current density profile to reduce q_0 at constant total current and constant edge current density.

6 ACKNOWLEDGMENTS

The authors have benefitted from numerous discussions with W.A.Cooper, G.Schultz, T.Tsunematsu and R.L.Dewar. This work was partly supported by the Swiss National Science Foundation.

7 REFERENCES

[1] C.M. Bishop et al., Nucl. Fusion 24 (1984) 1579

[2] C.M. Bishop et al., Nucl. Fusion 26 (1986) 1063

[3] T.Tsunematsu et al., Nucl. Fusion 27 (1987) 330

[4] C. Mercier et al.,Nucl. Fusion 27 (1987)149

[5] R. Gruber et al., Lausanne Report LRP 271/85 to appear in J. Comp.Phys.

[6] R.Gruber and J.Rappaz, Finite Elements Methods in Linear Ideal Magnetohydrodynamics (Springer-Verlag, Berlin-Heidelberg, 1985)

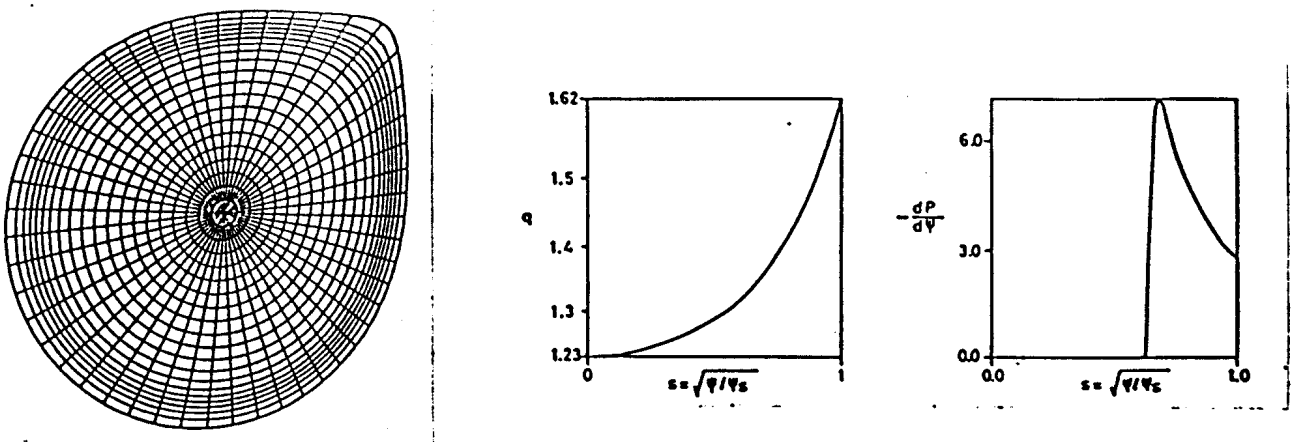

Fig.1 Flux surfaces, safety factor profile and marginal pressure gradient profile for a case without coalescence corresponding to $\alpha_o=45^o$, $\beta_p=0.26$, $\beta=1.46\%$, $I_E=0.5$ and $q_l=1.36$.

Fig.2 Dependence of ψ_c on total current and peaking factor of the current profile. Crosses show the maximum peaking alowable for the coalescence to occur at the plasma surface, this value is increasing with q_l (solid curves $\alpha_o=180^o$, broken curve $\alpha_o=90^o$ and $I_E=0.3$, dotted curve $\alpha_o=135^o$ and $I_E=0.3$).

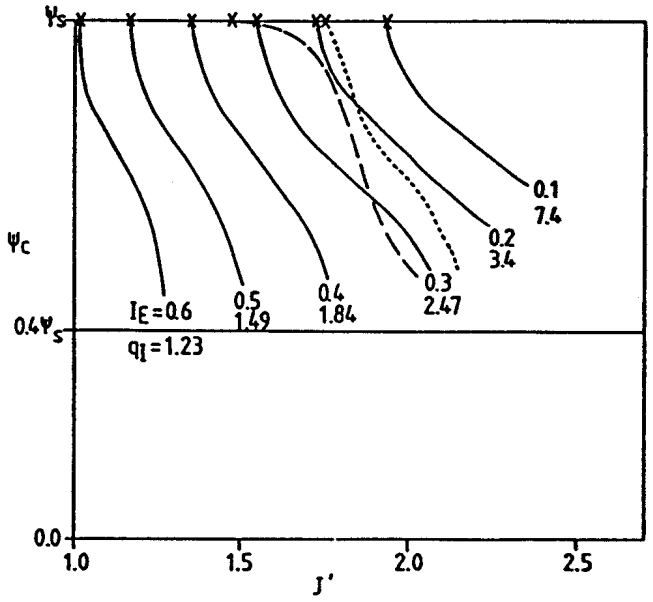

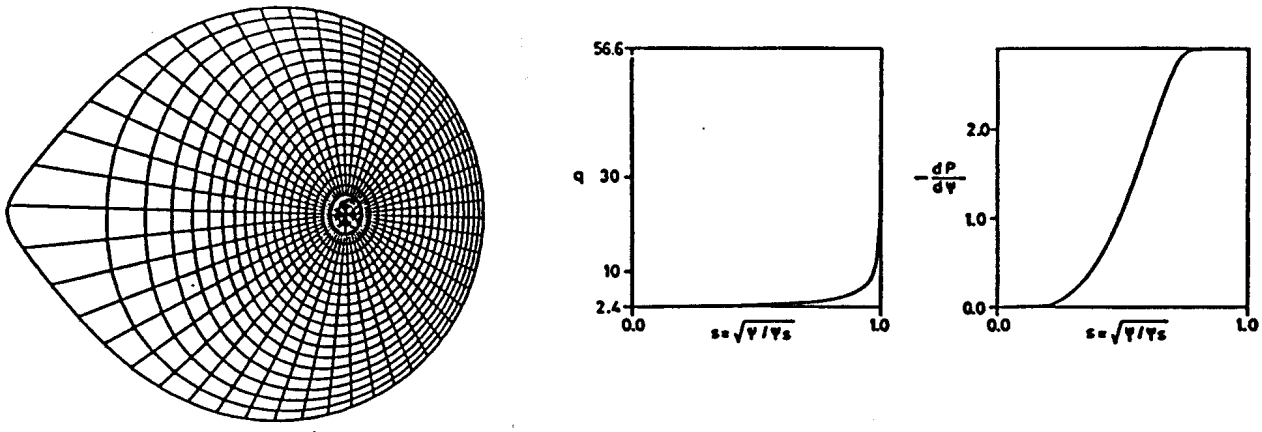

Fig.3 Flux surfaces, safety factor profile and pressure gradient profile of a case with an inside bump (α_o=180°) for β_p=2.95 , β=2.26% , l_E=0.2 and q_l=3.2 .

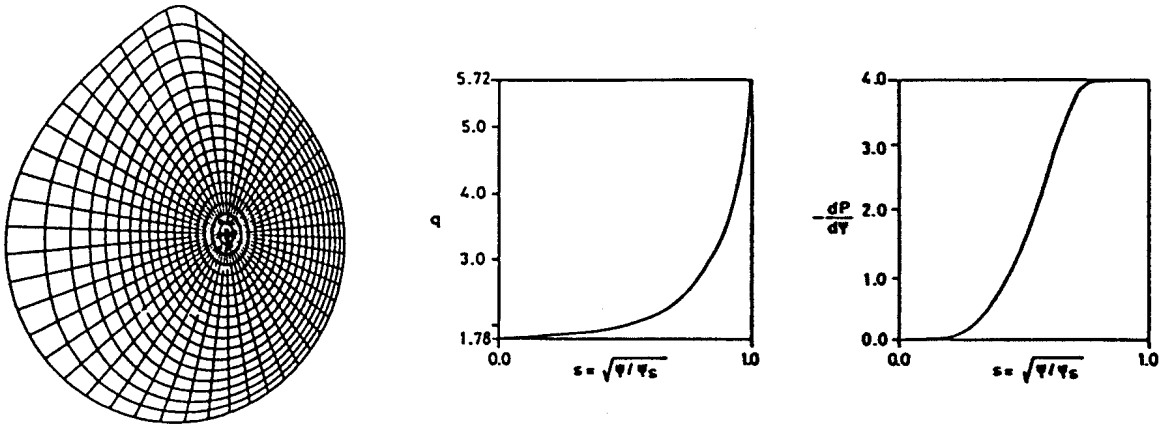

Fig.4 Same as Fig.2 but with α_o=90° , β_p=3.0 , β=5.57% , l_E=0.3 and q_l=2.1 .